JOURNAL OF MATERIALS SCIENCE **34** (1999) 691–700

Influence of calcination and sintering temperatures on the structure of $(Pb_{1-x}Ba_x)ZrO_3$

B. P. POKHAREL, M. K. DATTA, DHANANJAI PANDEY
School of Materials Science and Technology, Institute of Technology, Banaras Hindu University, Varanasi-221 005, India

$(Pb_{1-x}Ba_x)ZrO_3$ powders are synthesized below 800 °C for $x \leq 0.25$ using a semi-wet route involving solid-state thermochemical reaction in a mixture of ZrO_2 and $(Pb_{1-x}Ba_x)CO_3$. The $(Pb_{1-x}Ba_x)CO_3$ precursors were obtained by a "forced" coprecipitation technique. These powders can be sintered to achieve nearly 99% of the theoretical density at 1050 °C, which is 200 to 300 °C lower than that employed for the solid state route. The structure of as-calcined powder is orthorhombic for $x \leq 0.10$ and rhombohedral for $0.25 < x \leq 0.35$, whereas the two phases coexist for $0.15 \leq x \leq 0.25$. The structure of sintered material is orthorhombic for $0 \leq x \leq 0.10$, rhombohedral for $0.20 \leq x \leq 0.30$, and cubic for $x \geq 0.35$, whereas orthorhombic and rhombohedral phases coexist at $x = 0.15$. The difference in the structure of the as-calcined and sintered powders is discussed in terms of particle size effect and chemical homogenisation of Ba^{2+} in the PBZ matrix.

1. Introduction

Recent years have witnessed considerable interest in materials undergoing electric field induced antiferroelectric (AFE) to ferroelectric (FE) transitions accompanied by large volume expansion, which makes these materials potentially useful for actuator applications [1]. The AFE to FE transition in pure $PbZrO_3$ in the absence of biasing electric field occurs [2] just a few degree celsius below the FE to paraelectric (PE) transition temperature of 233 °C. In the presence of a biasing electric field, the AFE to FE transition temperature can be lowered [3], which may be explained by the fact that in the presence of biasing field, the free energy of the FE phase remains lower than that of the antiferroelectric phase over an extended range of temperatures. It has been shown [4–6] that the temperature range of the ferroelectric phase can be enhanced not only with increasing biasing field, but also by Ba^{2+} substitution. In fact, the AFE to FE switching can occur [6, 7] even at room temperature in $(Pb_{0.95}Ba_{0.05})ZrO_3$, whereas it requires much higher temperatures in pure $PbZrO_3$ [3].

The structure of the AFE phase is orthorhombic (A_O) with eight formula units in the unit cell [8, 9], whereas the FE phase has a rhombohedral structure (F_R) [7]. In the first comprehensive study on $(Pb_{1-x}Ba_x)ZrO_3$ (PBZ) system, Shirane and Hoshino [7] showed that the AFE(A_O) phase is stable at room temperature for $x \leq 0.15$, whereas the FE (F_R) phase is stabilized for $0.15 < x \leq 0.30$. On the other hand, Dutta [5] has shown that the structure is orthorhombic (A_O) for $x \leq 0.10$, rhombohedral for $x > 0.25$, while the two phases coexist for intermediate compositions, $0.10 < x \leq 0.25$, in powder samples of PBZ. More recently, Yoon *et al.* [6] reported that the room temperature structure of PBZ changes from orthorhombic to rhombohedral above $x = 0.25$. Although these workers do not explicitly discuss the coexistence of A_O and F_R phases, a perusal of their XRD patterns reveals that the two phases coexist for all compositions with $0.05 \leq x \leq 0.25$ and pure F_R phase is stabilized above $x = 0.25$. These findings are at variance with those reported by Shirane and coworkers [4, 7]. The present investigation was undertaken to settle this controversy about the room temperature structure of PBZ as a function of Ba^{2+} content for $0.05 \leq x \leq 0.35$.

Conventionally, $(Pb_{1-x}Ba_x)ZrO_3$ powders have been prepared by solid state thermochemical reactions in a particulate mixture of PbO, $BaCO_3$, and ZrO_2. In this dry route of synthesis, the reaction takes place in several steps, with $PbZrO_3$ formation at an early stage of the reaction followed by its conversion into $(Pb_{1-x}Ba_x)ZrO_3$, which involves long-range diffusion leading to frozen-in compositional inhomogeneities. Further, the completion of the reaction requires high temperatures ($\geq$1000 °C) [6, 10]. At such high temperatures, there is a possibility of evaporation of PbO [11]. Evaporation of PbO changes the materials properties due to the change of stoichiometry. For example, the temperature stability range of ferroelectric phase in $PbZrO_3$ has been reported [12] to be expanded by defects that could occur due to PbO evaporation. A lower calcination temperature ($\lesssim$800 °C) is always desirable because below 800 °C, PbO loss is negligible and yields finer powders with better reactivity leading to higher sintered densities at lower firing temperatures.

In the present work, $(Pb_{1-x}Ba_x)ZrO_3$ powders have been synthesized at temperatures $\lesssim$800 °C using a semi-wet route involving solid state thermochemical reaction between ZrO_2 and $(Pb_{1-x}Ba_x)CO_3$ solid solution precursors, where $(Pb_{1-x}Ba_x)CO_3$ solid solution

precursors were synthesized using chemical coprecipitation. This ensures uniform distribution of Ba^{2+} and Pb^{2+} ions in each particle of the precursor powder. In contrast to the conventional dry route where the typical separations between Ba^{2+} and Pb^{2+} ions are of the order of tens of thousands of Å, for micrometre size reactant particles, these ions are only a few unit cells apart, irrespective of the size of the precursor particles in the semi-wet route. This is expected to ensure uniform supply of Pb^{2+} and Ba^{2+} in the correct ratio at the unit cell level during the solid state thermochemical reaction with ZrO_2 particles, and hence, a homogeneous distribution of Pb^{2+} and Ba^{2+} ions in the final product. The advantages of using such a semi-wet method has been demonstrated in the synthesis of chemically homogeneous powders of (Ba, Ca)TiO_3 [13, 14], (Ba, Sr)TiO_3 [14, 15], PZT [16], 2223 phase in bismuth cuprate [17] and 123 phase in the Y-Ba-Cu-O system [18]. For PZT [16], (Ba, Ca)TiO_3 and (Ba, Sr)TiO_3 [14], it has been shown that the solid state thermochemical reaction temperature can be drastically lowered in the semi-wet route leading to sub-micrometer size powders.

2. Synthesis and characterization of $(Pb_{1-x}Ba_x)CO_3$

We have synthesized $(Pb_{1-x}Ba_x)ZrO_3$ compositions containing up to 35% barium ($x = 0.35$), which is at the border line of the composition showing ferroelectric behavior at room temperature. All of the samples were prepared using A.R. grade $BaCO_3$ and $PbCO_3$, with purity of 99.5% each. $PbCO_3$ and $BaCO_3$ powders mixed in desired molar ratios were dissolved in dilute nitric acid. $(Pb_{1-x}Ba_x)CO_3$ precursors were synthesized using a "forced" coprecipitation technique. In the conventional approach for the chemical coprecipitation of different cations in a multicomponent system, the pH at which each species precipitates out must be nearly identical. For our system, $BaCO_3$ precipitates out at a pH of about 8 whereas $PbCO_3$ was found to precipitate out at a pH of 3.5. As a result, if ammonium carbonate solution is added slowly to an acidic solution of lead and barium nitrates, the pH of the solution rises very slowly leading to the precipitation of $PbCO_3$ and $BaCO_3$ one after the other, defeating the very purpose of chemical route. To circumvent this problem, a concentrated solution of ammonium carbonate was added at a very fast rate to the acidic solution of lead and barium nitrates, while the solution was being stirred constantly. As a result, the pH of the solution rose almost instantaneously, leading to "forced" coprecipitation of $BaCO_3$ and $PbCO_3$. The filtrates were checked for the absence of Pb^{2+} and Ba^{2+} using dilute H_2SO_4, ammonia, and potassium dichromate solutions. The absence of Pb^{2+} and Ba^{2+} in the filtrates confirmed the complete precipitation of Pb^{2+} and Ba^{2+} present in the starting solutions. Precipitates were thoroughly washed with distilled water to remove excess ammonium carbonate and subsequently dried in an oven.

The formation of $(Pb_{1-x}Ba_x)CO_3$ solid solution was verified by X-ray diffraction using a 12 kW rotating anode X-ray diffractometer (Rigaku Rotaflex RTP 300 RC model), which was operated at 50 kV and 100 mA (5 kW). Fig. 1 depicts the X-ray diffraction patterns for $(Pb_{1-x}Ba_x)CO_3$ ($x = 0.05$, 0.10, 0.15, 0.20, 0.25, 0.30, and 0.35) prepared by "forced" coprecipitation technique. The absence of the most intense line of $BaCO_3$ at $2\theta = 24.1^\circ$ in all the diffractograms given in this figure not only confirms the forced coprecipitation of $BaCO_3$ and $PbCO_3$ but also indicates the formation of a solid solution of $BaCO_3$ and $PbCO_3$. The gradual addition of less concentrated ammonium carbonate solution does

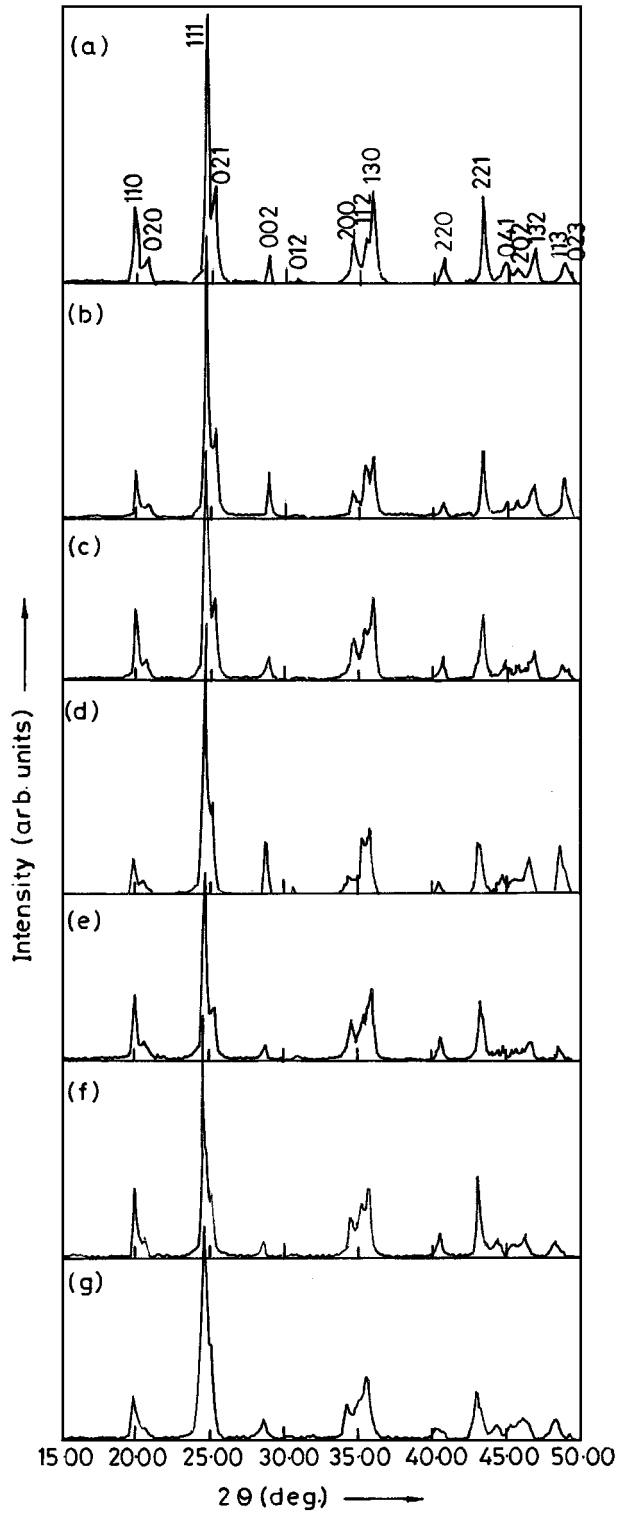

Figure 1 Powder diffractometer records of $(Pb_{1-x}Ba_x)CO_3$ precursor for (a) $x = 0.05$, (b) $x = 0.10$, (c) $x = 0.15$, (d) $x = 0.20$, (e) $x = 0.25$, (f) $x = 0.30$ and (g) $x = 0.35$.

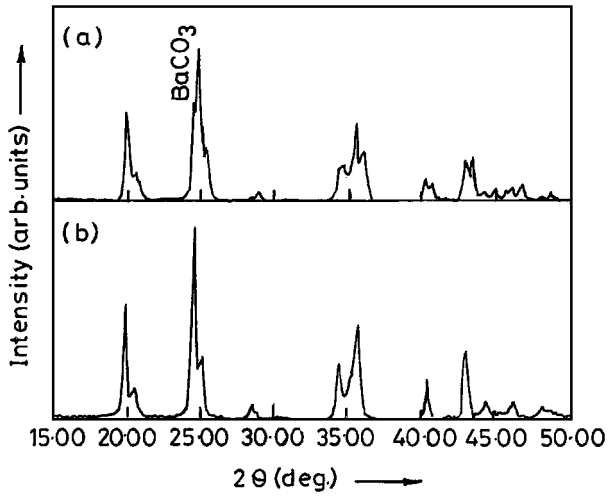

Figure 2 X-ray diffractogram of $(Pb_{0.75}Ba_{0.25})CO_3$ powders prepared by (a) normal precipitation and (b) "forced" coprecipitation showing the presence of $BaCO_3$ in (a).

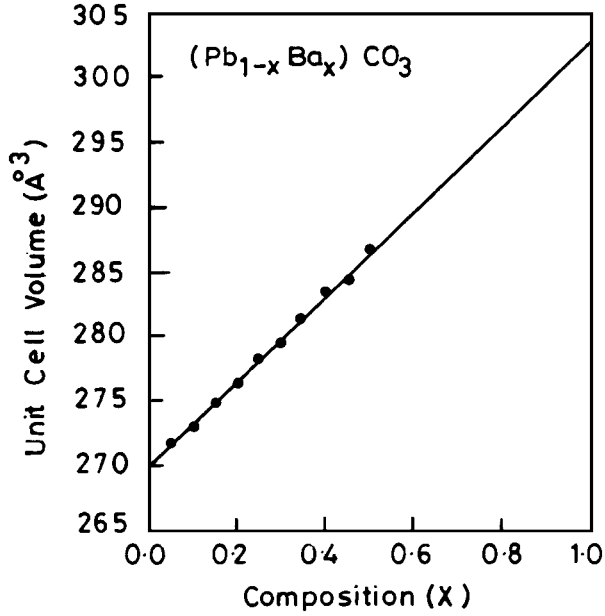

Figure 3 Unit cell volume of $(Pb_{1-x}Ba_x)CO_3$ as function of $BaCO_3$ content.

not lead to coprecipitation of $BaCO_3$ and $PbCO_3$, as can be seen from the X-ray diffractogram shown in Fig. 2, for a composition with $x = 0.25$. The presence of the characteristic $BaCO_3$ line at $2\theta = 24.1^\circ$ in Fig. 2 a clearly indicates that the $BaCO_3$ and $PbCO_3$ could not be coprecipitated on gradual addition of ammonium carbonate solution. The $BaCO_3$ reflection is absent in Fig. 2b, which corresponds to the "forced" coprecipitation.

It was possible to index all the diffraction lines in Fig. 1 with respect to an orthorhombic unit cell similar to that of $PbCO_3$. Table I lists the lattice parameters and unit cell volume of $(Pb_{1-x}Ba_x)CO_3$ precursors obtained by the least squares refinement method using reflections with $15^\circ \leq 2\theta \leq 60^\circ$. It is evident from Table I that the unit cell volume increases monotonically with increasing Ba^{2+} content. This is expected because the ionic size of Ba^{2+} (1.29 Å) is larger than that of Pb^{2+} (1.17 Å). This further confirms that Ba^{2+} has indeed entered into the $PbCO_3$ matrix. As shown in Fig. 3, the variation of the unit cell volume with Ba^{2+} content obeys Vegard's rule. The extrapolation of the line at $x = 0.00$ and 1.00 gives unit cell volumes of pure $PbCO_3$ and $BaCO_3$ as 268.98 and 303.57 $Å^3$, respectively, which is in good agreement with volume of $PbCO_3$ (270.70 $Å^3$) and $BaCO_3$ (304.24 $Å^3$) given in JCPDS files. All of these observations clearly confirm the solid solution formation in powders obtained by the "forced" coprecipitation technique. These solid solution precursor powders are expected to possess unit cell level uniform distribution of Pb^{2+} and Ba^{2+} ions in each powder particle irrespective of its size.

TABLE I Lattice parameters and unit cell volume of orthorhombic $(Pb_{1-x}Ba_x)CO_3$

x	a (Å)	b (Å)	c (Å)	V ($Å^3$)
0.05	5.180(1)	8.530(2)	6.151(1)	271.8(2)
0.10	5.182(3)	8.538(4)	6.168(3)	272.9(3)
0.15	5.198(2)	8.569(4)	6.171(3)	274.9(3)
0.20	5.216(3)	8.575(5)	6.178(4)	276.3(4)
0.25	5.227(1)	8.585(4)	6.202(3)	278.3(2)
0.30	5.229(2)	8.599(3)	6.215(2)	279.5(5)
0.35	5.251(2)	8.617(4)	6.237(3)	282.2(4)

3. Optimization of $(Pb_{1-x}Ba_x)ZrO_3$ formation temperature

For the synthesis of $(Pb_{1-x}Ba_x)ZrO_3$ powders, the precursor $(Pb_{1-x}Ba_x)CO_3$ powders were mixed with ZrO_2 (99.9% purity) in stoichiometric proportions. These mixtures were milled for six hours in a zirconia jar using a centrifugal ball mill. Acetone was used as the milling agent and zirconia balls were the grinding media.

We first optimized the calcination temperature for $x = 0.05$. The ball milled powders for $x = 0.05$ were calcined for six hours at 600 °C, 650 °C, and 700 °C in separate runs. Fig. 4a–c shows the XRD patterns of the calcined powders prepared at these temperatures. It is evident from the diffractogram for the powder calcined at 600 °C that the formation of $(Pb_{0.95}Ba_{0.05})ZrO_3$ has started at 600 °C (see the intense 110 perovskite peak in Fig. 4a). However, the reaction is quite slow since the powder contains substantial amount of unreacted PbO (yellow modification) and ZrO_2. At 650 °C, the reaction is faster because the perovskite peak is now much stronger than the peaks corresponding to PbO and ZrO_2 (see Fig. 4b) but the reaction is not completed in six hours. Calcination of the mixture of $(Pb_{0.95}Ba_{0.05})CO_3$ and ZrO_2 at 700 °C for six hours, on the other hand, yields powder that is single phase $(Pb_{0.95}Ba_{0.05})ZrO_3$ as is evident from the XRD pattern given in Fig. 4c. With increasing Ba^{2+} concentration, one requires higher calcination temperatures such as 735 °C for $x = 0.10, 0.15$, 760 °C for $x = 0.20$, 785 °C for $x = 0.25$, and 810 °C for $x = 0.30$ and 0.35. Thus, $(Pb_{1-x}Ba_x)ZrO_3$ powders up to $x \leq 0.25$ can be prepared at temperature $\lesssim$800 °C using the semi-wet route. As pointed out in the introduction, this low temperature synthesis is highly desirable to check the PbO loss, which becomes significant above 800 °C.

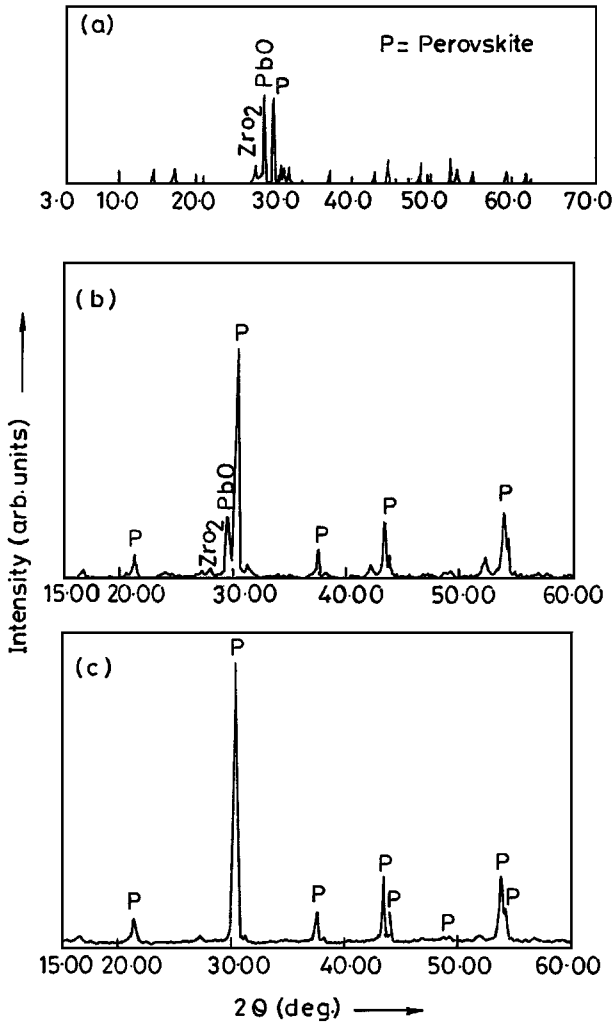

Figure 4 X-ray diffractograms showing the formation of $(Pb_{0.95}Ba_{0.05})ZrO_3$ at various calcination temperatures (a) 600 °C, (b) 650 °C and (c) 700 °C by semi-wet route.

In order to prepare PBZ powders under similar conditions at temperatures $\lesssim$800 °C, we chose 785 °C as the calcination temperature for all the compositions with $0.05 \leq x \leq 0.25$ and obtained single phase powders within six hours as shown in Fig. 5a–e. For $x = 0.30$ and 0.35, the calcination temperature was raised to 810 °C to get single phase powders within six hours as shown in Fig. 5f and g.

4. Comparison of calcination temperatures for semi-wet and dry routes

For a comparison with the conventional dry route, a mixture of 0.85PbO, $0.15BaCO_3$, and ZrO_2 was calcined at 785 °C for six hours. The calcined powder so obtained consists of PBZ, unreacted PbO, ZrO_2, and other unidentified phases in the XRD patterns as shown in Fig. 6a. The semi-wet route on the other hand can yield single phase powder even at 735 °C within six hours of calcination (see Fig. 6b). This shows that the formation of single phase $(Pb_{1-x}Ba_x)ZrO_3$ powders can occur at lower temperatures for the semi-wet route as compared to those for the conventional dry route. Apart from the lower temperature of synthesis, the semi-wet route is expected to give compositionally homogeneous powders because the uniform supply of Pb^{2+} and Ba^{2+} in the desired ratio at the time of reaction with ZrO_2 is always ensured at the unit cell level by the use of solid solution $(Pb_{1-x}Ba_x)CO_3$ precursors. This is not possible in the conventional dry route where the mixing of Pb^{2+} and Ba^{2+} in the reactant species is at the particulate level ($\sim 1\,\mu$m) in contrast to the unit cell level mixing in the semi-wet route. It is because of better chemical homogeneity that the 110 and 111 reflections of the perovskite phase near $2\theta = 30.3°$ and 37.4° are split in the Fig. 6b but not in Fig. 6a.

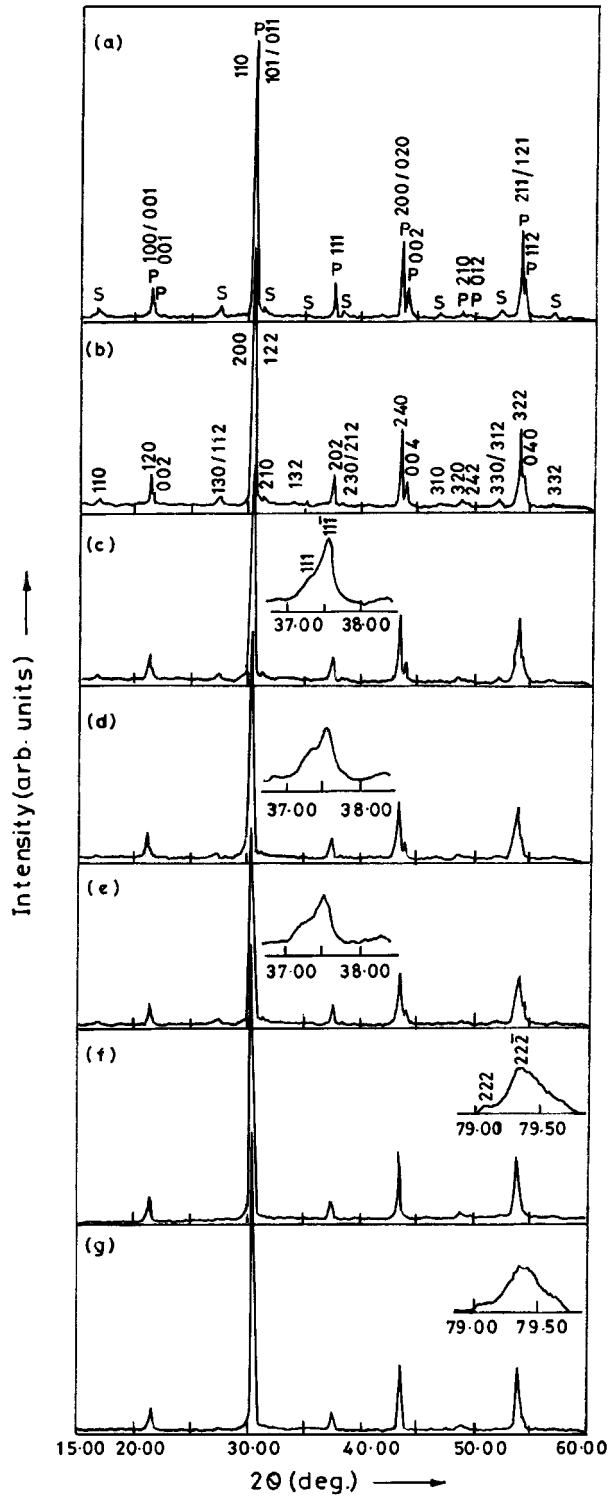

Figure 5 X-ray diffractograms of single phase PBZ powders obtained after calcination at 785 °C for (a) $x = 0.05$, (b) $x = 0.10$, (c) $x = 0.15$, (d) $x = 0.20$, (e) $x = 0.25$, and at 810 °C for (f) $x = 0.30$ and (g) $x = 0.35$.

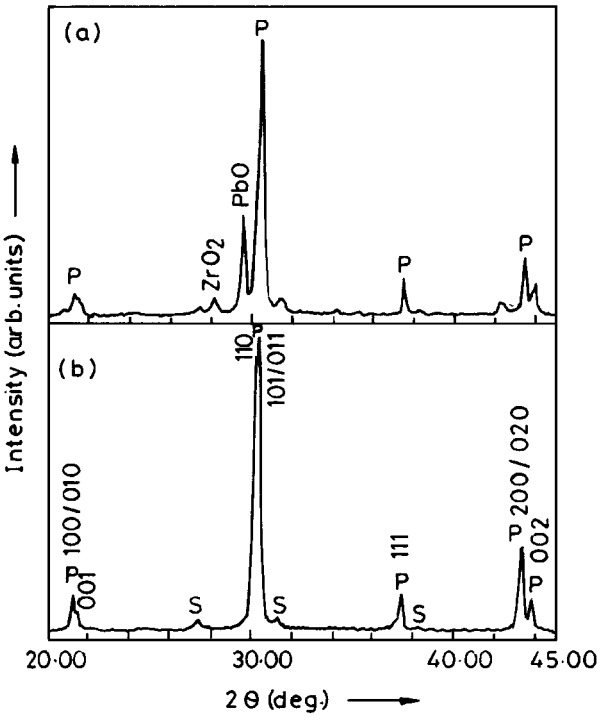

Figure 6 Comparison of calcination temperature for semi-wet and dry routes for obtaining single phase $(Pb_{1-x}Ba_x)ZrO_3$ powder for $x = 0.15$ (a) dry route calcined at 785 °C for 6 hours and (b) semi-wet route calcined at 735 °C for 6 hours.

5. Structure of as-calcined $(Pb_{1-x}Ba_x)ZrO_3$ powders

In the XRD patterns given in Fig. 5, the main perovskite reflections marked with P are distinguished from a set of relatively weak satellite reflections marked with S for $x \leq 0.25$. For $x > 0.25$ there are only perovskite reflections. The strong perovskite reflections can be indexed with respect to a tetragonal structure with indices 110/101, 111, 200/002, 210/201/102, and 211/112 as shown in Fig. 5a. The weak satellite reflections, however, cannot be indexed with respect to the simple tetragonal unit cell. To explain these, one has to postulate [9] a superlattice cell with orthorhombic symmetry. The orthorhombic cell parameters (a_O, b_O, c_O, and V_O) are approximately related to the elementary perovskite cell parameters (a_P, b_P, c_P, and V_P) in the following manner:

$$a_O \approx a_P\sqrt{2},\ b_O \approx a_P 2\sqrt{2},\ c_O \approx 2c_P \text{ and } V_O \approx 8V_P$$

For $x = 0.05$ and 0.10, all the diffraction lines could be indexed with respect to such an orthohombic superlattice cell. It is not possible to explain the splitting of cubic reflection 111 for $0.15 \leq x \leq 0.25$ and 222 for $x = 0.30$ and 0.35 using orthorhombic cell. The splitting of the cubic 111/222 reflections can be explained in terms of a rhombohedral distortion of the elementary perovskite cell [7]. For pure rhombohedral structure, 200 group of reflections should be a singlet. In Fig. 5, these reflections are also split for $0.15 \leq x \leq 0.25$, which is expected for the orthorhombic structure. This implies that there is a coexistence of rhombohedral and orthorhombic phases for the compositions $0.15 \leq x \leq 0.25$. For $x > 0.25$, the superlattice reflections and the splitting of the 200 group of reflections disappear, indicating the absence of the orthorhombic phase. The splitting of the cubic 111 and 112 group of reflections, on the other hand, confirms the rhombohedral symmetry of PBZ for $x > 0.25$.

Coexistence of rhombohedral and orthorhombic phases for $x = 0.15$, 0.20, and 0.25 can also be inferred from the relative intensity of 240 and 004 reflections of the orthorhombic phase. With increasing Ba^{2+} content, the ratio of intensities of these two sets of reflections gradually increases. In particular, the 004 reflection gradually becomes weaker with increasing x. In addition, calculations show that the interplanar spacing for the 200 reflection of the F_R phase nearly matches with that for the 240 reflection of the A_O phase. As a result, the 200 reflection of the rhombohedral phase is nearly superimposed on the 240 reflection of the orthorhombic phase causing the departure from the theoretically expected ratio for the orthorhombic phase for the intensity of 240 and 004 reflections. This implies that the fraction of the orthorhombic phase is decreasing with increasing Ba^{2+} content.

Table II lists the lattice parameters and unit cell volume of the orthorhombic and rhombohedral phases obtained by least squares refinement method using reflectios in the range $15^\circ \leq 2\theta \leq 80^\circ$. Fig. 7a and b depicts the variation of the cell parameters and until cell volume with barium content. For the orthorhombic phase, the variation of the equivalent elementary perovskite cell parameters (a_P, b_P, c_P and V_P) has been plotted. It is evident from this figure that a_R and V_R of the rhombohedral phase increase with increasing barium content especially for $x \geq 0.25$. This is expected because the size of Ba^{2+} is larger than that of Pb^{2+}. Surprisingly, the unit cell volume (V_P) of the orthorhombic phase does not exhibit a monotonic increase with barium content. V_P increases with barium content from $x = 0.05$ to $x = 0.10$ but for $x > 0.10$, it levels off. A similar variation is observed for c_P and a_P for $0.05 \leq x \leq 0.25$, whereas b_P is nearly independent of x.

TABLE II Lattice parameters and unit cell volume of as-calcined powders of $(Pb_{1-x}Ba_x)ZrO_3$

	Orthorhombic				Rhombohedral		
x	a_O(Å)	b_O(Å)	c_O(Å)	V_O(Å^3)	a_R(Å)	α(deg)	V_R(Å^3)
0.05	5.876(2)	11.756(4)	8.238(3)	569.1(1)			
0.10	5.886(1)	11.760(2)	8.252(1)	571.2(2)			
0.15	5.887(3)	11.756(4)	8.255(3)	571.3(3)	4.164(2)	89.76(5)	72.1(1)
0.20	5.885(2)	11.756(3)	8.253(2)	571.0(2)	4.164(4)	89.78(4)	72.1(2)
0.25	5.885(1)	11.761(3)	8.249(2)	570.9(1)	4.165(3)	89.80(5)	72.1(1)
0.30					4.170(1)	89.83(6)	72.4(1)
0.35					4.175(2)	89.86(5)	72.6(2)

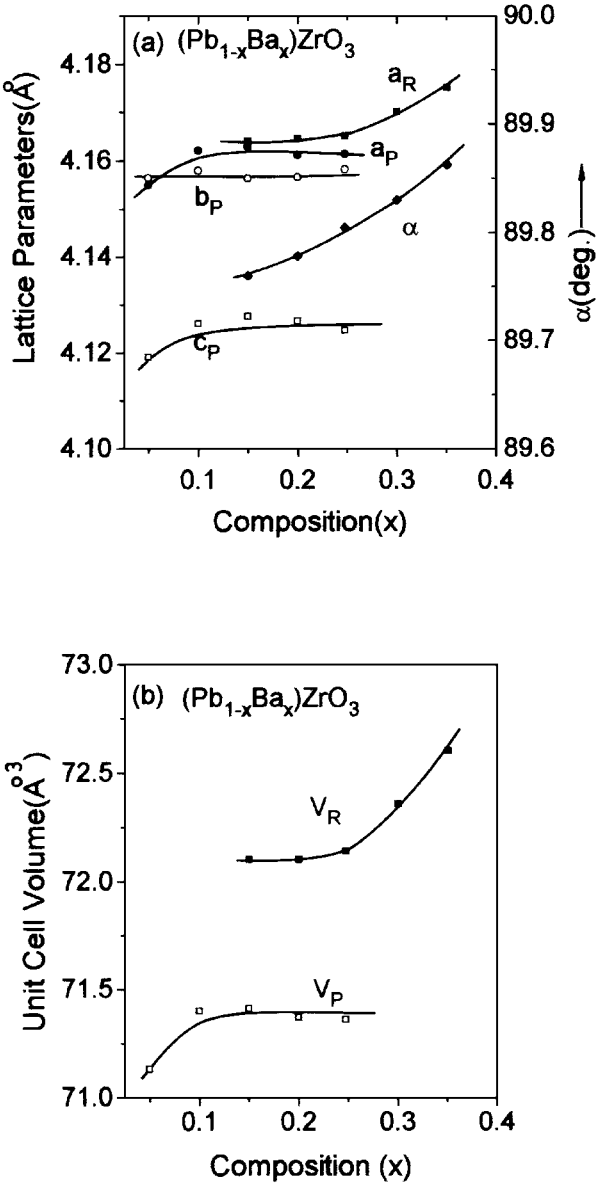

Figure 7 Variation of (a) unit cell parameters and (b) unit cell volume of as-calcined powders of $(Pb_{1-x}Ba_x)ZrO_3$ as a function of barium content.

6. Sintering of $(Pb_{1-x}Ba_x)ZrO_3$

For studying the structure of sintered PBZ powders, it was decided to calcine all of the compositions with $x \leq 0.35$ at 700 °C for six hours to minimize the PbO loss, which, as stated earlier, may become significant above 800 °C. The calcination at 700 °C was not sufficient for the completion of the PBZ formation, especially for higher barium compositions. However, it was found that the volatile component (CO_2) is completely removed after calcination at 700 °C for $x \leq 0.30$. For $x \geq 0.35$, it was not possible to completely get rid of the volatile component in six hours at 700 °C. These compositions ($x \geq 0.35$) were therefore recalcined at 850 °C in sealed PbO atmosphere to prevent the PbO loss. The calcined powders so obtained were mixed with a few drops of 2% solution of polyvinyl alcohol (PVA) as a binding agent and then compacted in the form of pellets in a steel die of 1.30 cm diameter using a hydraulic press at an optimized load of 80 KN. The green pellets were heated at 500 °C for 12 hours to burn off the binding agent (PVA). After burning off the PVA, PBZ pellets were sintered for three hours at an optimized temperature [5] of 1050 °C in covered platinum crucible with PbO atmosphere using $PbZrO_3$ as a spacer powder and MgO as a sealing agent to avoid the PbO evaporation from the samples at high firing temperatures.

TABLE III Percentage PbO loss, theoretical and bulk densities of sintered pellets for different barium content(x)

x	Theoretical Density (ρ_{th})	Bulk density (ρ_{bulk})	$(\rho_{bulk}/\rho_{th}) \times 100$	% PbO loss
0.05	7.952	7.935	99.79	0.20
0.10	7.850	7.818	99.59	0.21
0.15	7.720	7.676	99.43	0.22
0.20	7.625	7.577	99.37	0.18
0.25	7.541	7.489	99.31	0.22
0.30	7.439	7.386	99.29	0.26
0.35	7.344	7.262	98.89	0.24

The evaporation of PbO at higher sintering temperatures makes the task of maintaining the exact composition in $(Pb_{1-x}Ba_x)ZrO_3$ very difficult. Jona *et al*. [11] have shown that the percentage loss of PbO in $PbZrO_3$ after one hour at 1000 °C, 1100 °C, 1200 °C and 1300 °C can be 0.4, 3.5, 27.9, and 53.7, respectively. The use of low temperature (700 °C) for calcination and PbO atmosphere during sintering enabled the preparation of PBZ pellets with percentage weight loss less than 0.26, which is quite small. Table III lists the typical sintered densities and percentage PbO loss for various PBZ compositions. The density of the sintered pellets was measured using liquid displacement method. Glycerol of specific gravity 1.235 was used for this purpose. It is evident from this table that bulk densities close to or in excess of 99% of the theoretical density can be achieved at temperatures 200 ° to 300 °C lower using semi-wet derived powders as compared to those obtained by the dry route [4, 6]. Further, the PbO loss is very small in the sintered pellets. It is interesting to note that Yoon *et al*. [6] could achieve no better than 96–97% of the theoretical density even after sintering at much higher temperatures in the range 1200–1300 °C using PBZ powders obtained by the dry route. This shows that the powders derived by semi-wet route are highly reactive.

7. Structure of sintered powders

Powders obtained after crushing the sintered pellets of $(Pb_{1-x}Ba_x)ZrO_3$ prepared by semi-wet route were annealed at 550 °C for 6 h to remove strain induced during crushing before subjecting them to XRD analysis. Fig. 8 shows the diffractometer records for $(Pb_{1-x}Ba_x)ZrO_3$ with $x = 0.00$, 0.05, 0.10, 0.15, 0.20, 0.25, 0.30, and 0.35. The nature of XRD patterns for $x = 0.00$, 0.05, and 0.10 is qualitatively similar to that observed for the as-calcined powder. However, the reflections are sharper in Fig. 8 presumably due to the increase in the particle size after sintering. For $x = 0.15$, the cubic 111 reflection is split as expected for the F_R phase, but the 004 reflection of the A_O phase has not completely vanished. In addition, some of the superlattice reflections are still present. This suggests that both rhombohedral

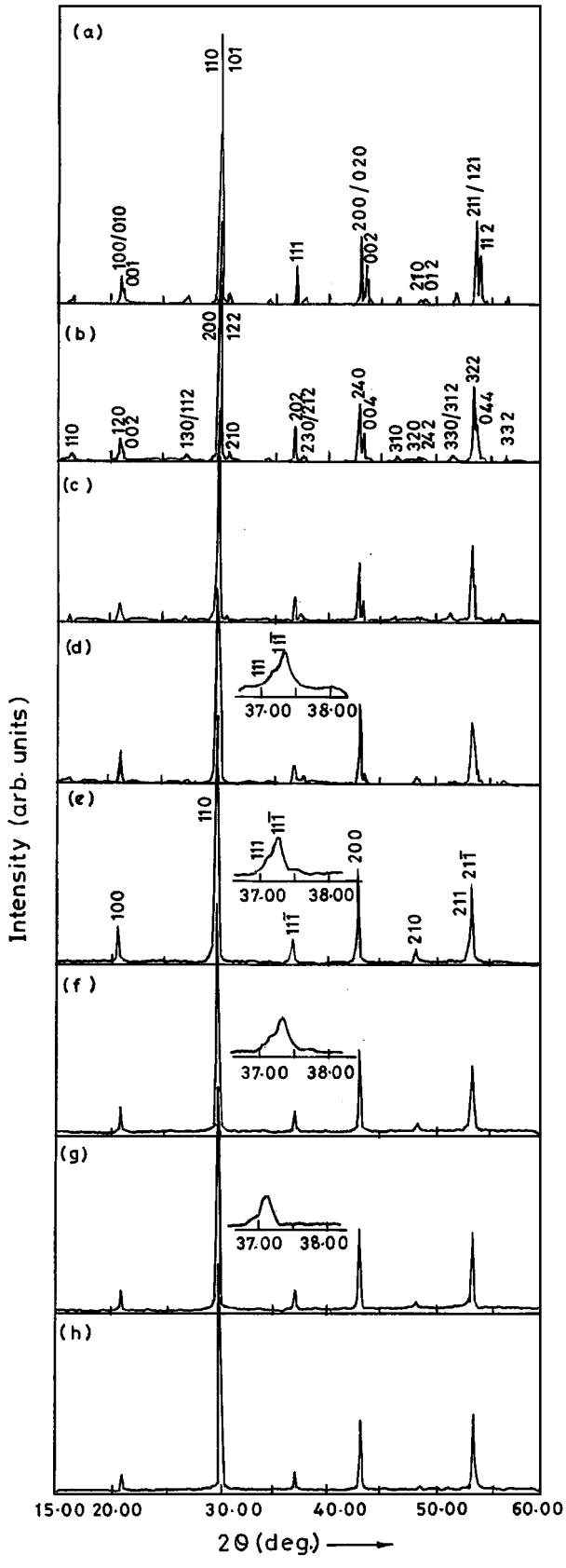

Figure 8 X-ray diffractograms of sintered powders of $(Pb_{1-x}Ba_x)ZrO_3$ for (a) $x = 0.00$ (b) $x = 0.05$, (c) $x = 0.10$, (d) $x = 0.15$, (e) $x = 0.20$, (f) $x = 0.25$, (g) $x = 0.30$ and (h) $x = 0.35$.

and orthorhombic phases coexist for this composition. Although a similar situation prevails for the as-calcined powder, the sintered powder is predominantly rhombohedral whereas the as-calcined powder has a significant proportion of the orthorhombic phase as evidenced by

TABLE IV Lattice parameters and unit cell volume of sintered powders of $(Pb_{1-x}Ba_x)ZrO_3$

	Orthorhombic			
x	a_O(Å)	b_O(Å)	c_O(Å)	V_O(Å^3)
0.00	5.884(2)	11.774(3)	8.225(2)	569.8(4)
0.05	5.887(2)	11.780(3)	8.236(2)	571.2(5)
0.10	5.891(1)	11.787(3)	8.260(2)	573.6(3)
0.15	5.893(2)	11.788(4)	8.296(3)	576.3(5)
	Rhombohedral			
x	a_R(Å)	α(deg)	V_R(Å^3)	
0.15	4.168(3)	89.81(4)	72.4(1)	
0.20	4.170(2)	89.84(5)	72.5(2)	
0.25	4.173(1)	89.88(3)	72.6(1)	
0.30	4.175(4)	89.94(2)	72.8(2)	
	Cubic			
x	a_C(Å)	V_C(Å^3)		
0.35	4.176(1)	72.8(2)		
0.40	4.178(3)	72.9(1)		
0.45	4.180(2)	73.0(2)		
0.50	4.182(2)	73.1(2)		

the relative intensity of the 240 and 004 reflections. For $0.20 \leq x \leq 0.25$, the superlattice lines of the orthorhombic antiferroelectric phase, which are present in the XRD patterns of the as-calcined powders, have vanished completely after sintering. In addition, the cubic 200 reflection, which was a doublet in the as-calcined powder, has now become a single whereas the cubic 111 reflection continues to remain a doublet for both the sintered and calcined powders. All of these clearly indicate that the structure is rhombohedral for $0.20 \leq x \leq 0.30$. For $x \geq 0.35$ the structure is cubic at room temperature (30 °C). Table IV lists the lattice parameters and unit cell volume obtained by least squares refinement using reflections in the range $15^\circ \leq \theta \leq 100^\circ$. The variation of the elementary perovskite unit cell parameters a_P, b_P, c_P and V_P for the orthorhombic phase with barium content in sintered PBZ samples is shown in Fig. 9a and b. It is evident from this figure that the difference between a_P and b_P is rather small, but even this small difference systematically decreases with increasing barium content up to $x = 0.15$. Similarly, the difference between c_P and a_P/b_P also decreases up to 0.15. Thus, the orthorhombicity decreases with increasing x and becomes zero somewhere between $x = 0.15$ and 0.20. The rhombohedral distortion (90-α) decreases with increasing x for $0.15\ x \leq 0.30$ and becomes zero for $x \geq 0.35$ when the structure becomes cubic. It is interesting to note that the unit cell volume increases with increasing x for all the three phases as expected on the basis of the larger ionic radius of Ba^{2+} compared to that for Pb^{2+}. In addition, there is a discontinuous change in volume for $0.15 < x \leq 0.20$ and $0.30 < x \leq 0.35$, corresponding to the change in the structure from A_O to F_R and F_R to P_C, respectively. The unit cell volume of the A_O phase is less than that of the F_R and P_C phases; the larger difference being between the volume of the A_O and F_R phases. These findings may appear to be similar to those of Shirane and Hoshino [7] with two significant differences. Shirane and Hoshino assumed

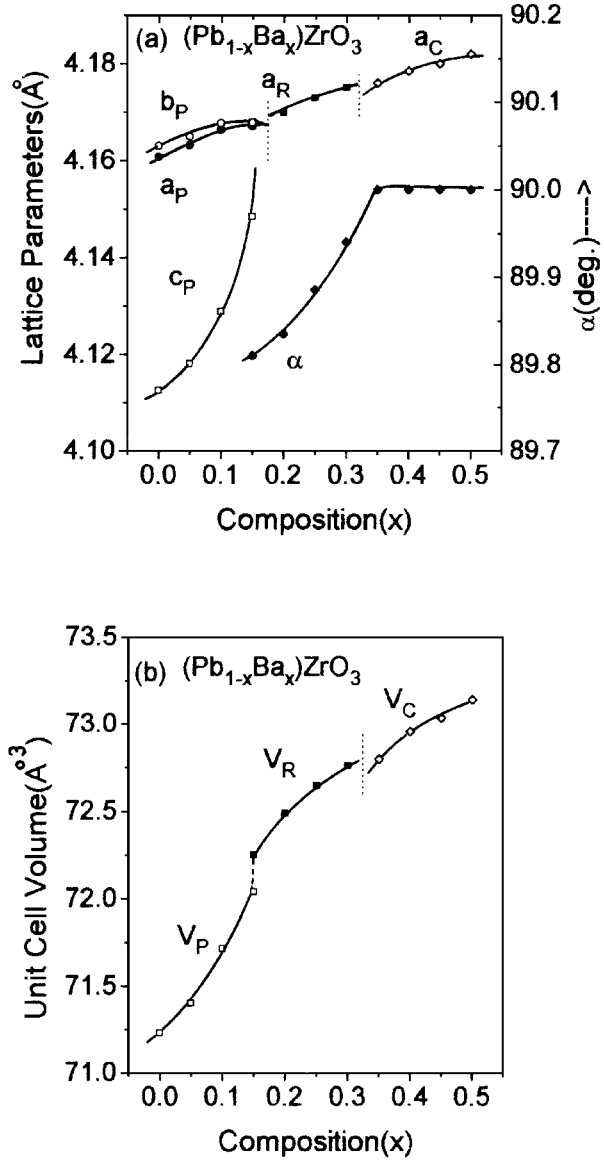

Figure 9 Variation of (a) unit cell parameters and (b) unit cell volume of sintered powders of $(Pb_{1-x}Ba_x)ZrO_3$ as a function of barium content.

a tetragonal unit cell for $x \leq 0.15$, which is not correct. In addition, they did not observe phase coexistence for $x = 0.15$.

8. Effect of calcination and sintering temperatures on phase coexistence

The results presented in the preceding sections show that A_O and F_R phases coexist for $0.15 \leq x \leq 0.25$ and $x = 0.15$ in the as-calcined and sintered powders, respectively. In both cases, lower barium content leads to the A_O phase while higher barium content stabilizes the F_R phase. This difference in the structure of the as-calcined and sintered powders may be due to several factors. The as-calcined powders are expected to be much finer than those obtained after sintering. One would like to verify if the A_O phase is getting stabilized in smaller size particles even though the structure of the bulk phase is rhombohedral for the same composition. The large volume difference (∼1%) between the orthorhombic and rhombohedral phases (see Fig. 7b) may make the nucleation of the A_O phase in the F_R matrix difficult because of the large strain energy. However, the A_O phase can easily nucleate at the surface of the powders where large volume changes can easily be accommodated. Because the particle size of the as-calcined powders prepared at 800 °C will definitely be much smaller than the size of the powders obtained after sintering at 1050 °C, the as-calcined powders will have effectively much more surface area where the A_O phase can easily nucleate. In addition, in the sintered pellets, the surface of all the grains other than those near the top and bottom faces is constrained by the surrounding grains, especially in dense ceramics such as the one in this study. As a result, the nucleation of the A_O phase may not occur easily inside the grains of sintered pellets except near the top and bottom faces of the pellets. This may account for the presence of the A_O phase over a wider composition range in the as-calcined powders.

This proposition can easily be verified by studying the structure of samples prepared at different temperatures because the particle/grain size will increase with increasing calcination/sintering temperatures. The results of such a study are shown in Fig. 10a, which depicts the XRD profiles of 240 and 004 reflections for $(Pb_{0.80}Ba_{0.20})ZrO_3$ prepared at 765, 800, 900, and 1050 °C in loose powder form. The heat treatments above 800 °C were carried out in PbO atmosphere to prevent any PbO loss. It is evident from this figure that the intensity of the 004 reflection decreases with increasing temperatures and becomes very low in powders prepared at 1050 °C. A similar trend was found in the sintered specimens of $(Pb_{0.80}Ba_{0.20})ZrO_3$ as shown in Fig. 10b for sintering temperatures of 900, 1050 and 1100 °C. The XRD patterns in Fig. 10b were recorded for powders obtained after crushing the pellets and then annealing the powders at 550 °C for six hours to remove any strains induced during crushing of the pellets. These observations tend to support our initial contention that with decreasing surface area by use of higher calcination or sintering temperature, the nucleation sites for the A_O phase decrease, and therefore, the relative amount of the F_R phase increases.

The effect of particle/grain size on the stability of ferroelectric phase is well known [19]. For example, in PZT ceramics, the cubic to rhombohedral distortion (90-α) increases with increasing particle size. However, for $(Pb_{0.80}Ba_{0.20})ZrO_3$, the rhombohedral distortion of the F_R phase decreases with increasing calcination/sintering temperature as shown in Fig. 11. In addition, the unit cell volume of the A_O phase increases with increasing calcination/sintering temperatures, as depicted in Fig. 11. The unit cell volume of the F_R phase also seems to increase with calcination/sintering temperatures but the difference in V_R at various temperatures is within the standard deviation as can be seen from Fig. 11. These observations cannot be explained in terms of grain/particle size effect and call for a separate explanation.

It appears that the use of higher calcination/sintering temperatures not only reduces the effective surface area due to grain growth but also leads to homogenisation of Ba^{2+} in the PBZ matrix This may appear surprising to begin with because the use of

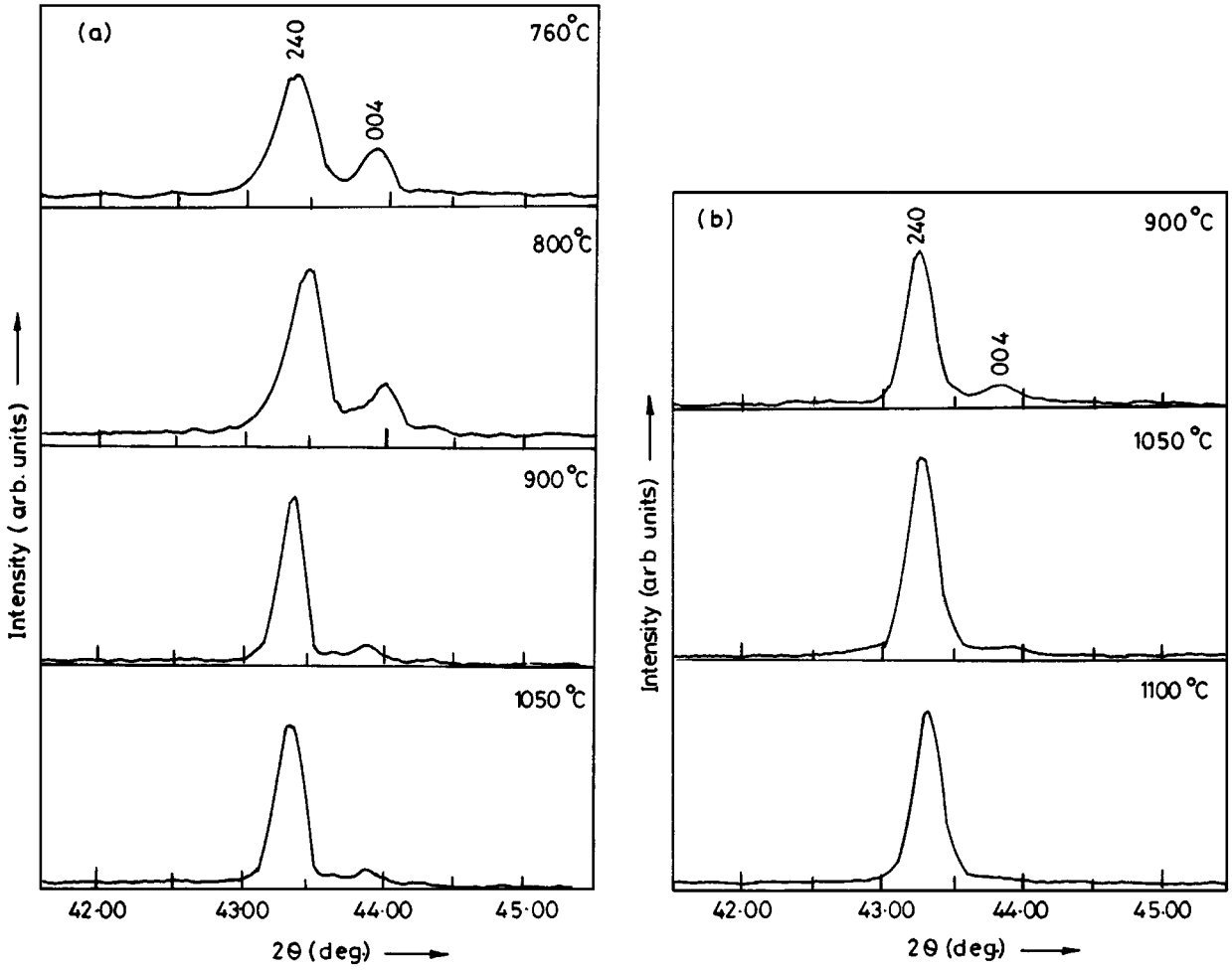

Figure 10 240 and 004 for XRD profiles of $(Pb_{0.80}Ba_{0.20})ZrO_3$ after (a) calcination at various temperatures in loose powder form and (b) sintering at various temperatures in pellet form.

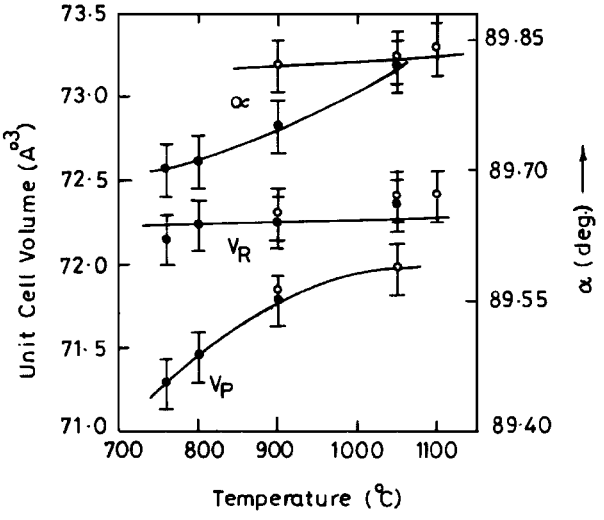

Figure 11 Variation of unit cell volume of orthorhombic and rhombohedral phases and rhombohedral angle with calcination/sintering temperatures for $(Pb_{0.80}Ba_{0.20})ZrO_3$: (●) calcined powders, (O) sintered pellets.

$(Pb_{1-x}Ba_x)CO_3$ solid solution precursor is expected to yield chemically homogeneous PBZ powders. However, if $(Pb_{1-x}Ba_x)CO_3$ precursors undergo entectoidal decomposition into lead-rich and barium-rich oxide phases before reacting with ZrO_2, the possibility of the formation of lead-rich PBZ and barium-rich PBZ cannot be ruled out at low calcination temperatures. With increasing calcination/sintering temperatures the lead-rich and barium-rich PBZ phases may diffuse into each other to give single phase homogeneous PBZ samples. The structure of lead-rich and barium-rich phases in $(Pb_{0.80}Ba_{0.20})ZrO_3$ are expected to be orthorhombic and rhombohedral, respectively. With increasing homogenization, the average barium content of the lead-rich PBZ phase will increase, and therefore, the volume of the orthorhombic phase will decrease. Only on completion of the homogenization, does one gets monophasic rhombohedral $(Pb_{0.80}Ba_{0.20})ZrO_3$ powders. The decrease in the rhombohedral distortion with increasing calcination/sintering temperatures, shown in Fig. 11, can also be attributed to the homogenization of Ba^{2+} because with increasing Ba^{2+} content, the rhombohedral distortion (90°-α) in sintered samples decreases as already shown in Fig. 9a.

9. Conclusions

1. The room temperature structure of $(Pb_{1-x}Ba_x)ZrO_3$ for $x < 0.35$ changes from orthorhombic to rhombohedral for higher barium composition.

2. The structure of PBZ powders prepared at temperatures $\leq 810\ ^\circ C$ is orthorhombic and rhombohedral for $0 \leq x \leq 0.10$ and $0.25 < x \leq 0.35$, respectively. Both these phases coexist for $0.15 \leq x \leq 0.25$.

3. The structure of PBZ powders obtained from pellets sintered at 1050 °C is orthorhombic and rhombohedral for $0 \leq x \leq 0.10$ and $0.20 \leq x \leq 0.30$, respectively. For $x = 0.15$, the two phases coexist and for $x \geq 0.35$ structure is cubic at room temperature.

4. The difference in the structure of the as-calcined and sintered PBZ powders is due to lack of homogeneous distribution of Ba^{2+} in PBZ powders prepared at lower temperatures as well as the smaller particle size of the as-calcined powders.

References

1. S. PARK, M. PAN, K. MARKOSKI, S. YOSHIKAWA and L. E. CROSS, *J. Appl. Phys.* **82** (1997) 1798.
2. L. GOULPEAU, *Sov. Phys.-Solid State* **8** (1967) 1970; B. A. SCOT and G. BURNS, *J. Am. Ceram. Soc.* **55** (1972) 331; R. W. WHATMORE and A. M. GLAZER, *J. Phys. C: Solid State* **12** (1979) 1505.
3. G. SHIRANE, E. SAWAGUCHI and Y. TAKAGI, *Phys. Rev.* **84** (1951) 476; J. HANDEREK, M. PISARSKI and Z. UJMA, *J. Phys. C: Solid State* **14** (1981) 2007.
4. G. SHIRANE, *Phys. Rev.* **86** (1952) 219.
5. M. K. DATTA, *Antiferroelectric and Ferroelectric Transitions in* $(Pb_{1-x}Ba_x)ZrO_3$ *System*, M. Tech. Thesis in Materials Technology, Banaras Hindu University, Varanasi (INDIA) (1995).
6. K. H. YOON, S. C. HWANG and D. H. KANG, *J. Mat. Sc.* **32** (1997) 17.
7. G. SHIRANE and S. HOSHINO, *Acta. Cryst.* **7** (1954) 203.
8. E. SAWAGUCHI, H. MANIWA and S. HOSHINO, *Phys. Rev.* **83** (1951) 1078.
9. F. JONA, G. SHIRANE, F. MAZZI and R. PEPINSKY, *ibid.* **105** (1957) 849.
10. S. ROBERTS, *J. Am. Ceram. Soc.* **33** (1950) 63.
11. F. JONA, G. SHIRANE and R. PEPINSKY, *Phys. Rev.* **97** (1955) 1584.
12. Z. UZMA, J. HANDEREK and M. PISARSKI, *Ferroelectrics*, **B4** (1985) 273.
13. V. S. TIWARI, N. SINGH and D. PANDEY, *J. Am. Ceram. Soc.* **77** (1994) 1813.
14. N. SINGH and D. PANDEY (To be published).
15. V. S. TIWARI, N. SINGH and D. PANDEY, *J. Phys.: Condens. Matter*, **7** (1995) 1441.
16. A. P. SINGH, S. K. MISHRA, R. LAL and D. PANDEY, *J. Mat. Sc.* **28** (1993) 5050.
17. D. PANDEY, A. K. SINGH and A. P. SINGH, *Physica C* 204 (1992) 179; D. PANDEY, A. K. SINGH, P. K. SHRIVASTAVA, A. P. SINGH, S. S. R. INBANATHAN and G. SINGH, *Physica C* **241** (1995) 279; D. PANDEY, S. S. R. INBANATHAN, P. K. SHRIVASTAVA, A. BANERJEE and G. SINGH, *Physica C* **261** (1996) 157.
18. D. PANDEY, V. S. TIWARI and A. K. SINGH, *J. Phys. D (Appl. Phys.)* **22** (1989) 182.
19. S. K. MISHRA and D. PANDEY, *J. Phys. Condens. Matter* **7** (1995) 9287.

Received 27 July
and accepted 26 August 1998